Deformation and in situ stress in the Nankai Accretionary Prism from resistivity-at-bit images, ODP Leg 196

L. C. McNeill,[1] M. Ienaga,[2] H. Tobin,[3] S. Saito,[4] D. Goldberg,[5] J. C. Moore,[6] and H. Mikada[4]

Received 8 October 2003; revised 24 November 2003; accepted 28 November 2003; published 17 January 2004.

[1] Borehole resistivity images from ODP Leg 196 allow rapid and complete qualitative assessment of deformation within the toe of the Nankai prism, Japan. Borehole breakouts were common within the prism but prominent in the trench-wedge unit around the frontal thrust, suggesting reduced sediment strength. Breakouts indicate consistent σ_2 orientations ($\sim$050°), compatible with northwesterly convergence. Deformation is dominated by discrete zones, including the frontal thrust and décollement zone. Prism fractures trend $\sim$NE–SW, consistent with convergence. The décollement shows minimal deformation and the dominant structural trend is $\sim$N–S. Prism deformation zones are characterized by high resistivity (compaction), whereas the décollement is apparently dilated, both with conductive fractures. Distribution of fracture orientations varies between log units confirming lithologic and rheologic influence. Pore pressure is elevated within the décollement and the misalignment of conductive fractures may reduce permeability. *INDEX TERMS:* 0915 Exploration Geophysics: Downhole methods; 5109 Physical Properties of Rocks: Magnetic and electrical properties; 8010 Structural Geology: Fractures and faults; 8045 Structural Geology: Role of fluids; 8164 Tectonophysics: Stresses—crust and lithosphere. **Citation:** McNeill, L. C., M. Ienaga, H. Tobin, S. Saito, D. Goldberg, J. C. Moore, and H. Mikada (2004), Deformation and in situ stress in the Nankai Accretionary Prism from resistivity-at-bit images, ODP Leg 196, *Geophys. Res. Lett.*, *31*, L02602, doi:10.1029/2003GL018799.

1. Introduction

[2] The accretionary Nankai margin, Japan, where the Philippine Sea Plate converges towards SW Japan and Eurasia (Figure 1), is the location of regular subduction earthquakes. The objectives of ODP Leg 196 (and Leg 190) were to evaluate physical properties of incoming sediments to a subduction zone and the relationships between fluid flow/pressure and deformation, the earthquake cycle and seismogenic zone development.

[3] Legs 131 and 190 [*Taira et al.*, 1991; *Moore et al.*, 2001a] drilled boreholes across the margin retrieving cores and wireline logs. Leg 196 drilled two of these sites, utilising state-of-the-art Logging While Drilling (LWD) to measure in situ physical properties [*Mikada et al.*, 2002]. The technique reduces problems associated with wireline logging in poorly consolidated sediments and records properties in their initial state. It also allows rapid determination of physical properties "on the fly", is unbiased by core recovery and avoids problems of sample reorientation. Coupled with ground truthing of cores, these data provide the ultimate tool in assessing deformation and physical properties in active margins.

[4] LWD data were collected at two sites (Figure 1), a reference site within the incoming basin section (1173) and a site penetrating the frontal thrust and décollement seaward of the seismogenic zone (808). This paper will focus on deformation and in situ stress determined from Resistivity at Bit (RAB) images at Site 808 which provide unparalleled imagery of borehole structure. Button electrodes provide resistivity images at three different depths beyond the borehole (1, 3, and 5"). The continuous 360° borehole image allows fractures, faults and bedding to be identified by contrasts in resistivity (a static-normalised plot indicates resistivity relative to the entire borehole range, therefore conductive features have less than average resistivity). Fractures can be quickly identified and recorded bypassing the laborious structural measurements and reorientation of core data. Borehole breakouts were common in Hole 808 and allow estimation and confirmation of in situ stress orientation. These are the first breakouts ever recorded from an accretionary prism and prove RAB imagery invaluable for stress analysis of less well studied active margins. Key issues to be investigated were (a) the distribution of deformation through the forearc, (b) variability of in situ stress from breakouts, (c) variability of fracture orientations and their relationship to regional stress and permeability, and (d) distribution of conductive versus resistive zones and fractures and their significance in terms of permeability and fluid flow.

2. RAB Imagery

[5] Drilling parameters enabled an $\sim$7.5 cm ($\sim$3″) vertical RAB image resolution, hence features <7.5 cm are irresolvable. Horizontal resolution is $\sim$6°, $\sim$1.5 cm for the $\sim$25 cm (9.9″) diameter borehole, decreasing beyond the borehole. Differentiation between fractures and bedding is only clearcut where the former cut or

[1]Southampton Oceanography Centre, University of Southampton, Southampton, UK.
[2]Ocean Research Institute, The University of Tokyo, Tokyo, Japan.
[3]Department of Earth and Environmental Science, New Mexico Institute of Mining and Technology, Socorro, New Mexico, USA.
[4]Deep Sea Research Center, JAMSTEC, Yokosouka, Japan.
[5]Borehole Research Group, Lamont-Doherty Earth Observatory, Columbia University, Palisades, New York, USA.
[6]Department of Earth Sciences, University of California, Santa Cruz, California, USA.

0094-8276/04/2003GL018799$05.00

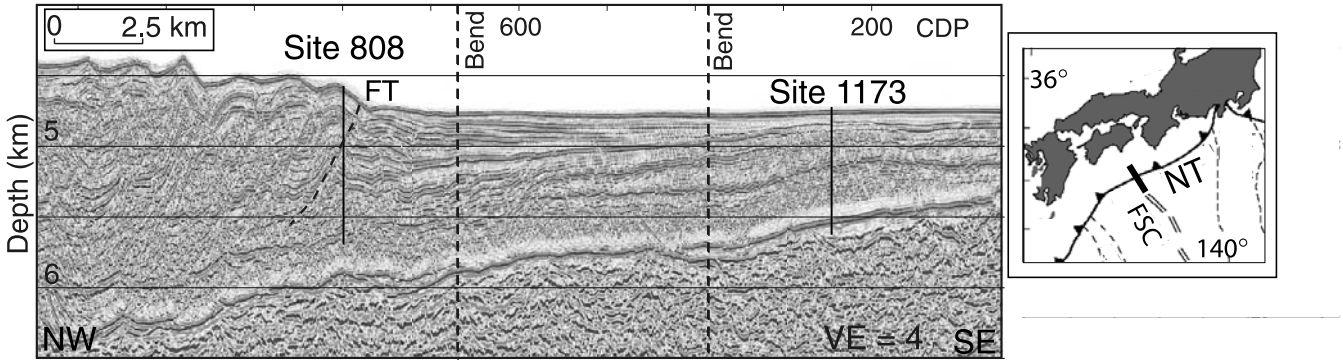

Figure 1. Seismic profile across Leg 196 sites [*Mikada et al.*, 2002]. Nankai Trough (NT) setting, line indicates profile. FSC = Fossil Spreading Centre; FT = frontal thrust.

displace the latter and fractures were identified by contrasting resistivity and dip. Image resolution is considerably less than in cores (mm's), e.g., fractures with no resolvable aperture or resistivity contrast cannot be imaged.

3. Nankai Accretionary Prism Deformation (808)

[6] The three main deformation zones (Figure 2) are (1) the frontal thrust zone (389–414 mbsf), (2) a densely fractured interval (559–574 mbsf) and (3) the décollement zone (937–965 mbsf) all correlating with Leg 131 cores [*Taira et al.*, 1991]. The fractured interval coincides with the base of the trench wedge unit suggesting lithological origin [*Taira et al.*, 1991], however its similarity to the frontal thrust zone supports a tectonic origin.

[7] On average, fracture orientations through the borehole show a NE-SW trend (Figures 2 and 3), as expected from the convergence vector of ~310–315° [*Seno et al.*, 1993]. Similar trends were observed in paleomagnetically-reoriented fractures from nearby Site 1174 [*Moore et al.*, 2001a].

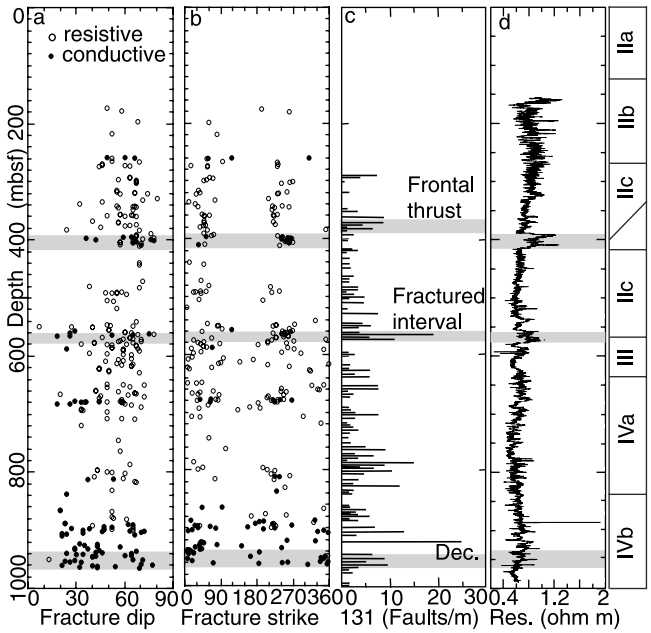

Figure 2. Interpreted 808 fractures from RAB images (a, b - strike as right hand rule) and Leg 131 cores (c). Resistive (open circles) and conductive (filled circles) fractures are indicated. Three major deformation zones are recognised: 1) frontal thrust zone; 2) fractured interval; and 3) décollement (Dec.). (d) Leg 196 resistivity data. Lithologic facies to right, [*Taira et al.*, 1991]. IIa, b U. and L. Axial trench; IIc Trench wedge; III Trench to basin; IVa, b U. and L. Shikoku basin.

4. Fracture Resistivity

[8] Conductive fractures dominate in the major deformation zones. Deformation between these zones is more sparse and dominated by resistive fractures (Figure 2). It is possible that "background" resistive fractures may be bedding planes or compactive shear zones [*Bourlange et al.*, 2003], but their orientations are still relevant to stress analysis.

[9] Prism deformation zones (1 and 2 above) are characterized by conductive fractures within zones of high resistivity (Figures 2 and 4). Conductive fractures probably represent open fractures but may represent fractures coated with pyrite, as tentatively identified on small faults by XRD analysis [*Taira et al.*, 1991]. The background resistive character of the zones suggests porosity collapse and

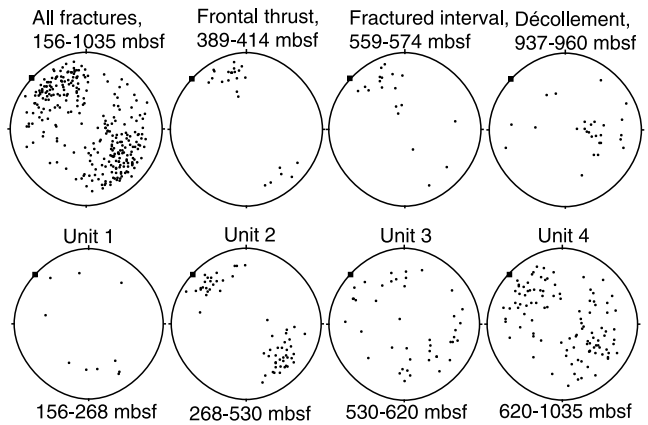

Figure 3. Equal area projections of poles to fracture planes at Site 808 from RAB images, square = convergence vector. The three main deformation zones and all fractures are shown. Second row shows fracture orientations within each log unit with fractures of the three main fault zones removed.

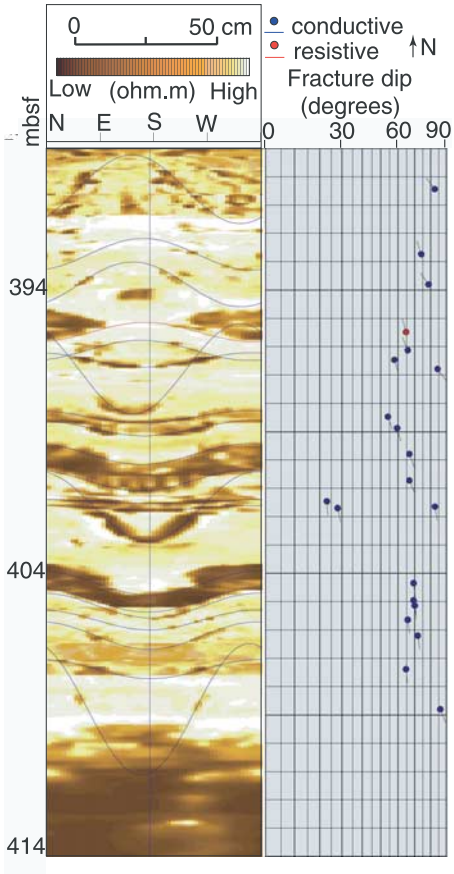

Figure 4. Static normalised RAB image of the frontal thrust zone. The unwrapped 360° image shows planar dipping fractures as sinusoids whose attitude is shown to the right of the image. Most fractures are conductive (dark) but the zone is resistive (light).

densification due to compactive deformation. Additional conductive fractures occur at ~680 mbsf without associated core fractures (Figure 2).

5. Frontal Thrust Zone

[10] This zone is the most deformed interval (Leg 196 and 131 data) and is characterised by high resistivity (Figures 2 and 4). Most fractures trend ENE-WSW (as do fractures in the fractured interval, 2), slightly deviating from the northwesterly convergence vector (Figure 3). Fractures exhibit a trend in dip direction, changing from north to south with depth, with the majority dipping south (Figure 3), suggesting antithetic fracturing associated with the NW-dipping fault zone. This trend is similar to folded bedding in Leg 131 cores, and may suggest that bedding planes have been misinterpreted as fractures. However, faults identified in the Leg 131 equivalent of the fractured interval (zone 2) are also antithetic [*Taira et al.*, 1991], supporting our initial interpretation.

6. Décollement Zone

[11] This zone is characterised by overall low resistivity, minor mottled higher resistivity zones (possible brecciation as in Leg 131 and 190 cores [*Taira et al.*, 1991; *Moore et al.*, 2001a]) and conductive fractures (Figure 2). The upper zone contact is ambiguous in RAB data relative to its clear equivalent in Leg 131 cores. Conductive fractures occur locally up to ~900 mbsf but the major fracture zone is 937–965 mbsf (Figure 2). Whereas prism fractures have an average ENE to NE trend consistent with the convergence vector and major structural trend, the dominant trend of décollement fractures is ~N–S (Figures 2 and 3). Leg 131 core measurements within the décollement [*Lallemant et al.*, 1993] show similar orientations to the prism (NE–SW). However, clusters of NNW-trending fractures occur immediately above the décollement zone within lithological unit IVb [*Lallemant et al.*, 1993]. Fractures within the décollement of nearby Site 1174 [*Moore et al.*, 2001a] show more variable trends than the prism but the average remains NE–SW.

7. Fracture Orientation With Depth and Lithology

[12] Fracture orientation was plotted for each of the log units and fault zones (Figure 3). Major changes in orientation occur between the fault zones and the intervening relatively undeformed sections. Fractures within deformation zones show clear trends and these fractures tend to be conductive. In contrast, ''background'' fracture orientation between deformed zones is more scattered and most are resistive (Figure 2). On average, each unit (with major deformation zones removed, therefore ''background'' fractures) exhibits fracture orientation consistent with the convergence vector. Unit 2 fracture poles cluster very tightly around the convergence vector, whereas Unit 3 and 4 poles are more scattered, with almost random orientation in Unit 3. This suggests lithological and physical property control of fracture orientation [e.g., *Finkbeiner et al.*, 1997].

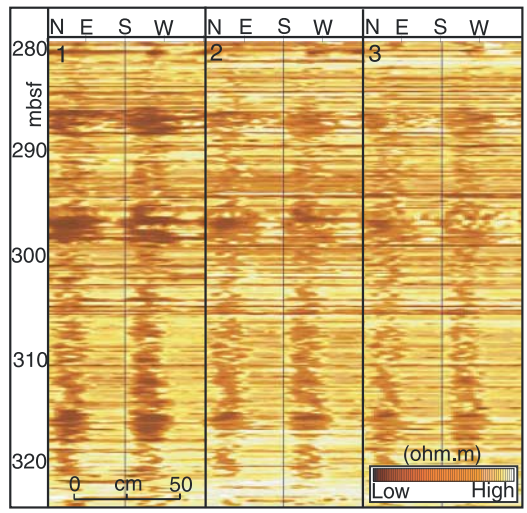

Figure 5. Static normalised RAB image within Unit 2. Borehole breakouts are two dark lines 180° apart representing borehole elongation in the direction NE-SW (σ_2). Three images represent resistivity 1" (1), 3" (2) and 5" (3) from borehole. Deformation decreases away from the borehole.

Unit 3 contains the fractured interval (zone 3) which contrastingly shows a strong WSW fracture trend.

8. Borehole Breakouts

[13] Breakouts form parallel to the minimum horizontal stress (σ_2) if vertical stress is nearly parallel to the borehole and tangential stress exceeds rock strength. Breakouts therefore give an indication of the current stress field. Breakouts were common throughout Hole 808 resulting from elongation of the borehole in the direction of σ_2 and appear as two conductive vertical lines 180° apart (Figure 5). A constant orientation is recorded ($\sim$050 ± 20°, NE-SW), which is as expected for the NW plate convergence vector parallel to σ_1. A similar σ_1 orientation (305–315°) was determined from inversion of fault clusters in Leg 131 cores [*Lallemant et al.*, 1993]. These results confirm previous measurements of σ_1.

[14] Continuous breakouts are recorded $\sim$270–530 mbsf, coincident with Log Unit 2 (Lithologic Unit IIc), bracketing the frontal thrust zone (Figure 2). Rheology may change between units and compressive sediment strength of Unit 2 may be reduced. Lith. Unit IIc is characterised by fine grained turbidites of the trench wedge [*Taira et al.*, 1991], Unit IIb above contains coarse grained sediments whereas III marks increased ash layers with clays and silts. Lithologic control on fissility and shear band production was also suggested for Leg 131 cores, where shear bands decrease in abundance at $\sim$550–560 mbsf at the base of Lith. Unit IIc [*Taira et al.*, 1991]. These bands may be related to brittle-ductile shear [e.g., *Karig and Lundberg*, 1990]. Lithological control of deformation bands in shallower sediments of nearby Site 1174 was also suggested [*Moore et al.*, 2001a]. Breakouts may alternatively be related to the stress regime around the frontal thrust zone. Breakouts continue below 530 mbsf but are intermittent, and none are observed within the décollement.

9. Discussion

9.1. Décollement Fracture Orientation

[15] The anomalous fracture orientation within the décollement may indicate development of different types of fractures within the same stress field (presumed NW σ_1 but unconfirmed below the plate boundary) caused by physical properties and diagenetic processes, rotation or stress heterogeneities. Alternatively, the stress regime may change across the décollement or fractures may be inherited from an existing fabric in the incoming sediment section. The fossil spreading centre of the incoming basin trends $\sim$NNW (Figure 1) and is a possible origin for $\sim$N-S trending fractures. Fracturing within the décollement may be isolated from or complexly related to the current prism stress field, a preferred hypothesis.

9.2. Fractures, Resistivity and Fluid Flow

[16] A reverse-polarity seismic reflection across the décollement [*Moore and Shipley*, 1993], reflects an increase in porosity [*Screaton et al.*, 2002]. Waveform modelling suggests variable character of the décollement zone itself with velocities/densities locally lower than overlying strata possibly due to fluid pressure [*Moore and Shipley*, 1993]. RAB resistivity data show a trend of decreasing resistivity (Figure 2d) and increasing porosity through the décollement zone, in addition to high porosity underlying the zone [*Bourlange et al.*, 2003]. Coupled with low porosity core material [*Taira et al.*, 1991; *Moore et al.*, 2001b], *Bourlange et al.* [2003] suggest a compacted décollement fault zone with dilatant fractures, although core properties may represent isolated clasts rather than bulk properties. Overpressures suggest that sediment permeability is insufficient to allow fluid expulsion [*Screaton et al.*, 2002]. Long term fluid budgets suggest a zone of transient fluid flow within and/or below the décollement zone [*Saffer and Bekins*, 1998], but flow is minor relative to likely diffuse flow through the prism.

[17] Average resistivity trends from Leg 196 data across the frontal thrust, fractured interval (560 mbsf) and décollement suggest that the two former are densified (high resistivity) whereas the décollement is dilated (low resistivity) (Figure 2d). Fractures within all three major zones are conductive. These observations prompt several questions: (1) Are conductive fractures open and are they related to permeability and fluid flow? (2) Fractures differ in orientation between prism fault zones and the décollement zone - how does fracture orientation and aperture correlate with the regional stress field and permeability [*Barton et al.*, 1995; *Finkbeiner et al.*, 1997]?

[18] (1) Fracture orientation within the frontal thrust zone is broadly as expected from regional stress as indicated by breakouts, and therefore consistent with fractures being active and open (?), supported by high conductivity (Figure 4). Seafloor seeps suggest fluid flow along faults within the forearc. (2) Elevated pore pressure within and below the décollement [*Moore and Shipley*, 1993; *Bourlange et al.*, 2003] may result from reduced permeability, which in turn, may be linked to the misalignment of fractures, although the stress regime is unconfirmed here. Elevated pore pressure may cause these fractures to be open and conductive but not associated with fluid flow.

10. Summary

[19] RAB imagery has proven invaluable for rapid deformation and stress analysis in active margins. Borehole resistivity images collected during Leg 196 at the toe of the Nankai prism were analysed, producing the following observations: (1) consistent breakout orientations indicate a uniform stress field through the prism, but their occurrence is influenced by lithology and physical properties; (2) variable fracture orientations may reflect stress heterogeneities, lithology, or rotation; and (3) RAB images indicate deformation zones of dilation and compaction which may correlate with pore pressure and potentially fluid flow, where data are consistent with an overpressured and low permeability décollement zone.

[20] **Acknowledgments.** This research used data provided by the Ocean Drilling Program (ODP). ODP is sponsored by the U.S. NSF and participating countries under management of Joint Oceanographic Institutions (JOI), Inc. Tobin and Moore are supported by USSSP grants USSSP-196-F0014 and F001431-F001464, respectively. We thank the crew and participants of ODP Leg 196. This paper benefited from the comments of J. Morgan, D. Saffer and two anonymous reviewers. McNeill acknowledges the Royal Society for support.

References

Barton, C. A., M. D. Zoback, and D. Moos (1995), Fluid flow along potentially active faults in crystalline rock, *Geology*, *23*, 683–686.

Bourlange, S., P. Henry, J. C. Moore, H. Mikada, and A. Klaus (2003), Fracture porosity in the décollement zone of Nankai accretionary wedge using Logging While Drilling resistivity data, *Earth Planet. Sci. Lett.*, *209*, 103–112.

Finkbeiner, T., C. A. Barton, and M. D. Zoback (1997), Relationships among in-situ stress, fractures and faults, and fluid flow: Monterey Formation, Santa Maria Basin, California, *AAPG Bull.*, *81*, 1975–1999.

Karig, D. E., and N. Lundberg (1990), Deformation bands from the toe of the Nankai accretionary prism, *J. Geophys. Res.*, *95*(B6), 9099–9109.

Lallemant, S. J., T. Byrne, A. Maltman, D. Karig, and P. Henry (1993), Stress tensors at the toe of the Nankai accretionary prism: An application of inverse methods to slickenlined faults, in *Proc. Ocean Drilling Prog.*, *Sci. Res.*, 131, edited by I. A. Hill, A. Taira, J. V. Firth et al., pp. 103–122, College Station, Texas.

Mikada, H., K. Becker, J. C. Moore, A. Klaus, et al. (2002), *Proc. Ocean Drilling Prog.*, *Init. Rep.*, 196 (CD-ROM), College Station, Texas.

Moore, G. F., and T. H. Shipley (1993), Character of the décollement in the Leg 131 area, Nankai Trough, in *Proc. Ocean Drilling Prog.*, *Sci. Res.*, 131, edited by I. A. Hill, A. Taira, J. V. Firth et al., pp. 103–122, College Station, Texas.

Moore, G. F., A. Taira, and A. Klaus, et al. (2001a), *Proc. Ocean Drilling Prog.*, *Init. Rep.*, 190 (CD-ROM), College Station, Texas.

Moore, G. F., et al. (2001b), New insights into deformation and fluid flow processes in the Nankai Trough accretionary prism: Results of Ocean Drilling Program Leg 90, *Geochem., Geophys., Geosys.*, *2*, doi:10.1029/2001GC000166.

Saffer, D. M., and B. A. Bekins (1998), Episodic fluid flow in the Nankai accretionary complex: Timescale, geochemistry, flow rates and fluid budget, *J. Geophys. Res.*, *103*(B12), 30,351–30,370.

Screaton, E., D. Saffer, P. Henry, S. Hunze, et al. (2002), Porosity loss within the underthrust sediments of the Nankai accretionary complex: Implications for overpressures, *Geology*, *30*, 19–22.

Seno, T., S. Stein, and A. E. Gripp (1993), A model for the motion of the Philippine Sea plate consistent with NUVEL-1 and geological data, *J. Geophys. Res.*, *98*(B10), 17,941–17,948.

Taira, A., I. Hill, J. Firth, et al. (1991), *Proc. Ocean Drilling Prog.*, *Init. Rep.*, 131, College Station, Texas.

L. C. McNeill, Southampton Oceanography Centre, University of Southampton, Southampton, SO14 3ZH, UK. (lcmn@soc.soton.ac.uk)

M. Ienaga, Ocean Research Institute, The University of Tokyo, Tokyo, Japan.

H. Tobin, Department of Earth and Environmental Science, New Mexico Institute of Mining and Technology, Socorro, NM, USA.

S. Saito and H. Mikada, Deep Sea Research Center, JAMSTEC, Yokosouka, Japan.

D. Goldberg, Borehole Research Group, Lamont-Doherty Earth Observatory, Columbia University, Palisades, NY, USA.

J. C. Moore, Department of Earth Sciences, University of California, Santa Cruz, CA, USA.